Sensors and Actuators Reports 11 (2026) 100464

Contents lists available at ScienceDirect

Sensors and Actuators Reports

journal homepage: www.sciencedirect.com/journal/sensors-and-actuators-reports

# A comparison of inkjet-printed amperometric and transistor-based biosensors towards continuous glucose monitoring

Federica Mariani [a], Francesca Ceccardi [a], Giulia Casula [b], Andrea Falchi [a], Luca Sartorelli [a], Giulia Costa [a], Isacco Gualandi [a], Piero Cosseddu [b], Annalisa Bonfiglio [c], Stefano Lai [b,*], Erika Scavetta [a,1,*]

[a] Department of Industrial Chemistry "Toso Montanari", University of Bologna, Via Piero Gobetti 85, 40129 Bologna, Italy
[b] Department of Electrical and Electronic Engineering, Cagliari, Piazza d'Armi, 09123, Italy
[c] University School for Advanced Studies (IUSS), Piazza della Vittoria 15, 27100 Pavia, Italy

ARTICLE INFO

*Keywords:*
Flexible electronics
Organic electrochemical transistor
Glucose sensor
Amperometric sensor
Ink-jet printing

ABSTRACT

Continuous glucose monitoring (CGM) is a technologically challenging topic, whose global medical relevance drives research efforts in several scientific fields. In this study, we analyze the potential of fully-ink-jet printed, flexible electrochemical biosensors for glucose monitoring with particular emphasis on the systematic comparison between two complementary device architectures. Specifically, amperometric and organic electrochemical transistor (OECT) structures entirely made of ink-jet printed poly(3,4-ethylenedioxythiophene):poly(styrene sulfonate) (PEDOT:PSS) are equipped with a biosensing interface modified with Pt nanoparticles and a membrane immobilizing glucose oxidase, where glucose is detected through the oxidation of hydrogen peroxide. The analytical performance of the two sensing configurations is systematically evaluated upon miniaturization, guiding the adjustment of both printing and functionalization strategies. Morphological, electrochemical and electrical characterizations are used to investigate the transduction mechanisms, characterize the key performance indexes and highlight the advantages of each sensing structure. On one hand, the intrinsic amplification provided by the transistor architecture results in higher sensitivity in the micromolar range (12 vs 0.43 mA $M^{-1}$, for OECT and amperometric sensors respectively). On the other hand, the lower S/N ratio exhibited by the OECT negatively impacts on the detection limit (66 μM for the transistor and 18 μM for the amperometric sensor). Overall, both sensor types are promising for the real-time glucose monitoring in biofluids like saliva and extracted interstitial fluid. Moreover, the miniaturized ink-jet printed devices outperform current state-of-the-art ink-jet printed glucose biosensors, most of which are not fully printed and flexible, or do not include the immobilized enzyme-containing layer in a compact layout.

## 1. Introduction

Self-monitoring blood glucose (SMBG) has revolutionized the field of diabetology and is the most widespread practice in the prevention and daily management of diabetes. However, the growing role of artificial intelligence and personalized medicine in our society, together with the raising awareness in the use of continuous glucose monitoring (CGM) devices, suggest that there is significant room for innovation. On one hand, blood self-testing has established the integration of electrochemical sensors in our everyday life and remains unmatched among the current approaches in terms of accuracy and simplicity, but, on the other hand, it is uncomfortable, invasive and only provides discontinuous monitoring, which stand as the major drawbacks [1]. In this view, there is a growing interest in the development of minimally invasive/non-invasive wearable platforms enabling continuous, real-time monitoring of the dynamic glucose concentration, which is demonstrated by the massive and continuous release of research contributions and reviews focusing on this topic [1–6]. Among the easily accessible biofluids containing glucose, such as sweat and saliva, interstitial fluid (ISF) has emerged due to its clinical relevance (good correlation with blood glucose concentration) and commercially available, minimally invasive CGM devices mainly rely on it [2,5].

* Corresponding authors at: Department of Electrical and Electronic Engineering, Cagliari, Piazza d'Armi, 09123, Cagliari, Italy.
*E-mail addresses:* stefano.lai@unica.it (S. Lai), erika.scavetta2@unibo.it (E. Scavetta).
[1] Prof. Erika Scavetta – Department of Industrial Chemistry "Toso Montanari", University of Bologna, Via Piero Gobetti 85, 40129 Bologna, Italy.

https://doi.org/10.1016/j.snr.2026.100464
Received 6 November 2025; Received in revised form 12 March 2026; Accepted 26 March 2026
Available online 27 March 2026
2666-0539/© 2026 The Authors. Published by Elsevier B.V. This is an open access article under the CC BY license (http://creativecommons.org/licenses/by/4.0/).

The successful design of body-compliant wearable platforms entails continuous research progress in fabrication techniques [6,7], where the low cost and the use of soft, lightweight and flexible materials are not only essential to address the requirements of point-of-care conformable devices, but also have a large impact on the robustness of the electrochemical sensing interface from an electrochemical point of view. Overall, the realization of large-area wearable sensors with high uniformity, stability and device yield poses several challenges in thin films deposition, patterning, processing, and functionalization [7]. Printing technologies are emerging for sensing applications, as they include less expensive procedures than lithography and are compatible with a wider variety of substrates and electrode materials, though reaching lower resolution [8]. Compared to other printing techniques such as screen-printing, spray and aerosol-jet printing, ink-jet printing offers several advantages, as it is a contactless, stencil-free, and material-efficient approach with superior resolution capabilities, allowing the digital fabrication of customizable designs under ambient conditions [9]. The performance of electrochemical sensors is largely affected by the physical properties of the active layer, which are in turn dictated by the deposition technique. Compared to screen-printing, ink-jet printing allows for precise control over layer thickness through drop spacing and multiple print passes, thus enabling tailored optimization of the sensor performance. Moreover, more homogeneous electrode surfaces can be obtained with higher roughness and porosity, thus improving reproducibility and leading to a higher electrochemically active area [10].

Among ink-jet printable active materials, organic semiconductors are quite popular thanks to their low cost, solution-processability and versatility [11]. In an interesting paper, a multisensing platform was presented for the amperometric detection of glucose, lactate and triglycerides based on a polyaniline hydrogel formed in-situ after ink-jet printing of the precursors on the working electrode. The sensing interface was completed via analogous in-situ formation of Pt nanoparticles (NPs), ink-jet printing of the enzymes solutions and final enzymes immobilization [9]. Nevertheless, the authors made use of prescreen-printed carbon paste and Ag/AgCl electrodes on polyethylene terephthalate (PET) and the platform was validated using serum samples, as its linear response is not suitable for glucose determination within naturally secreted biofluids for non-invasive sensing. A widely used organic semiconductor for ink-jet printed glucose biosensors is poly (3,4-ethylenedioxythiophene):poly(styrene sulfonate) (PEDOT:PSS), which is commercially available in aqueous dispersions and it is biocompatible, highly conductive and stable compared to other conjugated polymers, and can be easily functionalized via physical and (electro)chemical routes [8]. One of the first examples of ink-jet printed PEDOT:PSS based amperometric glucose biosensors was obtained upon subsequent printing of the organic semiconductor ink and the enzyme solution, then protected using a cellulose acetate membrane [12]. However, this printed prototype, including solely the working electrode, was realized on a rigid substrate (ITO glass) and only characterized with a redox mediator in solution. More recently, a fully ink-jet printed PEDOT:PSS biosensor was fabricated on paper, with glucose oxidase (GOx) and redox mediator printed on the working electrode [13]. Despite its proof of concept application to saliva samples, the use of bare PEDOT:PSS pseudo-reference and counter electrodes raises concerns about the reliability of the analytical signal and the analytical figures of merit are not clearly provided.

Alternative to the conventional amperometric approach, PEDOT:PSS is also the most employed semiconductor for the realization of Organic Electrochemical Transistors (OECTs) based sensors, which are regarded as a major emerging technology in the area of flexible electronics in the last decades [8]. Thanks to the characteristic volumetric doping promoting high modulation under low operating voltages, OECT-based sensors can combine signal transduction and amplification for specific sensing events, ranging from redox reactions to electrostatic interactions [7]. Despite the lower maturity compared to amperometric sensors, OECT based sensors show high versatility in adapting to unconventional architectures and substrates [14–16] and enable easy manufacturing procedures, particularly thanks to the absence of reference/pseudo-reference elements in their typical structure. In a recent publication, a printed OECT sensor was fabricated on a cellulose acetate film and PEDOT:PSS was ink-jet printed to form the transistor channel, while carbon-based source, drain and gate were realized by blade coating [17]. Gate and drain potentials were optimized based on the maximum transconductance to +0.7 and −0.8 V, respectively, while glucose detection was only carried out in a mixture of phosphate buffer and GOx confined on the OECT through the use of a containment well. To the best of our knowledge, a single example of fully ink-jet printed OECT sensor for glucose detection was reported in literature [18]. The device has a graphene gate electrode to facilitate charge transfer in the presence of glucose and a PEDOT:PSS channel; the sensing behavior is analyzed with the enzyme either in solution and immobilized around the gate electrode. However, only in the former condition and in the presence of a redox mediator (ferrocene), the sensor shows good linearity and comparable performance with state-of-the-art OECT sensors fabricated using lithography processes on rigid substrates.

In this manuscript, the design and miniaturization of fully-ink-jet printed devices based on PEDOT:PSS on flexible substrates are discussed and their functionalization is optimized in view of non-invasive glucose sensing applications. Specifically, we analyze the performance of amperometric and transistor structures through the lenses of electrochemistry and engineering, providing a detailed investigation on the transduction mechanism and functionalization of the sensing interface, as well as on the printing strategies developed to improve robustness and sensing performance. Upon device miniaturization, the resulting biosensors outperform the sensitivities reported for other ink-jet printed OECT/amperometric sensors described to date for glucose detection.

## 2. Materials and methods

### 2.1. Chemicals and buffers

Bovine serum albumin (BSA) / > 96 %, D-(+)-Glucose, monobasic potassium phosphate ($KH_2PO_4$), Glucose oxidase from aspergillus niger, Glutaraldehyde solution $C_5H_8O_2$ 25 wt. % in $H_2O$, Hexachloroplatinic acid hydrate ($H_2PtCl_6 \bullet H_2O$) 99.9 %, Potassium chloride KCl > 99 % and Potassium hydroxide (KOH) were purchased from Sigma Aldrich. The phosphate buffer solution (PBS) was prepared with 0.1 M $KH_2PO_4$ and adjusted to pH 7.00 with 1 M KOH. Hydrochloric acid (HCl) 37 % wt. was bought from ACS reagents and Silver nitrate ($AgNO_3$) 99.8 % from Acros Chimica. 5 nm Pt nanoparticles in ultrapure water (2 mg/mL) were purchased from DropSens.

### 2.2. Apparatus

All electrochemical and electrical experiments were carried out with a CH Instruments 660C potentiostat and a Keysight B2902A Source Measure Unit (SMU). Atomic Force Microscopy (AFM) measurements were obtained by means of a Scanning Probe Microscopy (SPM) SOLVER PRO by NT-MDT in semi-contact mode using NT-MDT NSG01 tips.

### 2.3. Devices fabrication

A 250-μm-thick polyethylene naphthalate (PEN, Goodfellow) substrate was employed for the fabrication of all devices studied in this work, e.g., electrodes, OECTs and amperometric sensors. The fabrication process is identical for all realized structures, and it is mainly based on large-area techniques, e.g., ink-jet printing and chemical vapor deposition (CVD). At first, a 2 μm-thick Parylene C buffer layer was deposited by CVD on PEN substrates using a PDS 2010 Labcoater 2 (Specialty Coating System). An oxygen plasma treatment was then performed on Parylene C surfaces to enhance their hydrophilicity and wettability, and

improve adhesion. Indeed, in order to ensure high conductivity of electrical connections, Ag tracks were patterned by means of inkjet printing through a Dimatix Materials Printer DMP2830 (Fujifilm Dimatix). Specifically, a 16-nozzle cartridge with a single drop volume of 10 pL (DMC-11,610, Fujifilm Dimatix) was filled with a silver nanoparticle-based ink (Cabot conductive Ink 300, Cabot), filtered through a 0.45 μm PTFE syringe filter. Silver tracks printing was performed using one nozzle with a firing voltage of 30 V, a drop spacing of 30 μm was set, the cartridge and the platen were kept at room temperature. The printed films were annealed in oven for 20 min at 150 °C in order to sinter the silver ink. PEDOT:PSS (PJET HC, Heraeus, Germany) electrodes were printed using a 16-nozzle cartridge with a single drop volume of 1 pL (DMC11601, Fujifilm Dimatix). In particular, the ink was sonicated in an ultrasound bath for 30 min and subsequently filtered with a 0.45 μm PTFE filter prior to filling the cartridge. Three nozzles, biased with a firing voltage of 30 V, were employed for printing electrodes defined by the overlap of four subsequently printed layers. A drop spacing of 20 μm was set, and the printer platen was maintained at a fixed temperature of 60 °C. A curing step over a hot plate at 90 °C for 15 min was performed as post-processing of PEDOT:PSS electrodes. Subsequently, an encapsulation layer, consisting of a 1.3 μm-thick Parylene C film, was deposited by CVD on the whole structure. In order to expose PEDOT:PSS sensing areas, selective Parylene C removal was performed by means of oxygen plasma etching. Two extra PEDOT:PSS layers were inkjet printed on the sensing areas after Parylene C removal, employing the same PEDOT:PSS-filled cartridge ink and the same printing parameters described before. A final post-processing over a hot plate at 90 °C for 15 min was performed.

A total number of 96 OECTs and 72 amperometric devices was fabricated, with different geometrical features. The overall process yield, intended as devices actually electrically measurable, was about 90 % for OECTs and 97 % for amperometric devices, considering all possible investigated geometries. Reproducibility within a single device batch, intended as the 3-σ tolerance band of resistance values at the longer conductive line (i.e., the channel in OECTs and the counter electrode in amperometric devices) among devices printed using the same cartridge, was of about 13 % for OECTs and 11 % for amperometric devices. Inter-batch reproducibility, considered as the relative standard variation of the same average resistance among different batches, was 12 % for OECTs and 25 % for amperometric devices.

### 2.4. Functionalization of the sensing interfaces

Platinum(Pt)-black was electrodeposited by applying a −0.2 V vs SCE for 180 s on a PEDOT:PSS working electrode (WE), in an three-electrode cell setup by using a Pt wire as a counter electrode (CE) and a saturated calomel electrode (SCE) as a reference electrode (RE) containing a 5 mM Hexachloroplatinic acid solution in diluted hydrochloric acid, obtained by dissolving $H_2PtCl_6 \bullet H_2O$ in 0.05 M HCl. The drop cast volume depends on the target area, which must be fully covered with the enzyme solution before being dried in air. For the final, miniaturized devices, 2 μL of 1 U/μL GOx were drop cast on the electrode surface. The enzyme is then immobilised by drop casting a suitable volume of a 3:1 mixture of 4 mg/mL BSA and glutaraldehyde (25 wt. % in $H_2O$) in order to fully cover the modified surface. The electrodes were left at room temperature until dry (a few minutes) and then placed in the fridge at 4 °C inside a closed container with a damp atmosphere. The deposition of Ag/AgCl was carried out in a three-electrode cell equipped with a Pt wire and a SCE. At first, Ag NPs were deposited by applying a −0.2 V for 30 s to the PEDOT:PSS electrode in a 0.1 M $AgNO_3$ solution. The modified PEDOT:PSS surface is then washed with distilled water and a Ag/AgCl composite is formed by applying +0.6 V for 30 s in a 1 M KCl solution.

### 2.5. Characterization

The electrochemical characterization was performed via cyclic voltammetry with a classical three-electrode cell setup. The PEDOT:PSS/Pt/GOx-GA-BSA electrode was exploited as a working electrode and potentials were applied against a SCE while using a Pt wire as a counter-electrode. The electrodes were immersed in a conventional electrochemical cell containing 0.1 M PBS (pH 7.00) and the current was recorded during the addition of different amounts of glucose to the electrolyte within an applied potential window ranging from - 0.2 V to 0.7 V at 50 mV/s. OECTs were characterized upon acquisition of output and transfer curves in 0.1 M PBS (pH 7.00) by applying drain (Vd) and gate (Vg) voltages and measuring the drain (Id) and gate (Ig) currents. Output curves were recorded at a scan rate of 10 mV/s with Vg from −0.5 to 0.6 V, Vd from −0.5 to 0.5 V, while transfer curves were recorded with Vg from −0.5 to 0.5 V and Vd equal to - 0.2 V.

### 2.6. Glucose sensing

The glucose response of amperometric sensors was evaluated via amperometry upon application of +0.65 V vs SCE or 0.45 V vs their pseudo-reference electrode in a cell containing 0.1 M PBS (pH 7.00). To conduct the test, once a stable baseline current is obtained, controlled volumes of 0.1 M glucose are added to the stirred electrolyte using a micropipette. The steady-state current is the analytical signal that correlates with the analyte concentration. For the OECT sensors, potentiostatic measurements were carried out maintaining fixed Vd of - 0.2 V and Vg of +0.8 V and recording Id while adding different amounts of 0.1 M glucose solution to 0.1 M PBS (pH 7.00) under magnetic stirring. The steady-state drain current is the analytical signal that correlates with the analyte concentration. The sensitivity to glucose is expressed as the slope of the least squares linear fitting of current value vs glucose concentration, while the correlation between the current values and the glucose concentrations is expressed by the $R^2$ coefficient of determination (COD). Detection limit (LOD) values were calculated using the 3σ/m criterion (where σ is the standard deviation of the blank and m is the slope of the calibration curve).

## 3. Results

### 3.1. Optimisation of the biosensing interface

The functionalization protocol optimized to form the transducer interface on PEN flexible substrates is schematically reported in Fig. 1a. First of all, the ink-jet printed PEDOT:PSS electrode was electrochemically modified upon Pt deposition using a traditional three-electrode cell configuration; subsequently, a controlled amount of the enzyme was drop-cast on the surface and therefore immobilized upon deposition of a BSA/GA membrane. Fig. 1b shows the voltammograms of the resulting biosensor recorded in 0.1 M PBS when increasing glucose amounts were added to the electrolyte solution contained in the three-electrode cell. The shape of the voltammograms clearly changes as glucose concentration increases, thus suggesting the occurrence of redox phenomena. The absence of well-defined faradaic peaks is in accordance with previously reported characterizations of ink-jet printed PEDOT:PSS biosensors [12], where the large capacitance of the semiconductor dominates. Evident faradaic contribution only appears in the case of biosensors modified with a redox mediator [13]. Considering these diagnostic experiments, a potential of +0.65 V SCE was chosen to carry out amperometric measurements in a standard three-electrode cell and define the analytical performance of our biosensor during glucose detection (Fig. 1c). Glucose concentration was varied from 10 to 1250 μM in the electrolyte solution under stirring and the recorded current exhibits stepwise increases as a consequence of the analyte additions over time. The steady-state signal linearly correlates with glucose concentration (Fig. 1c, inset) and the obtained sensitivity is 18 mA $M^{-1}$ $cm^{-2}$.

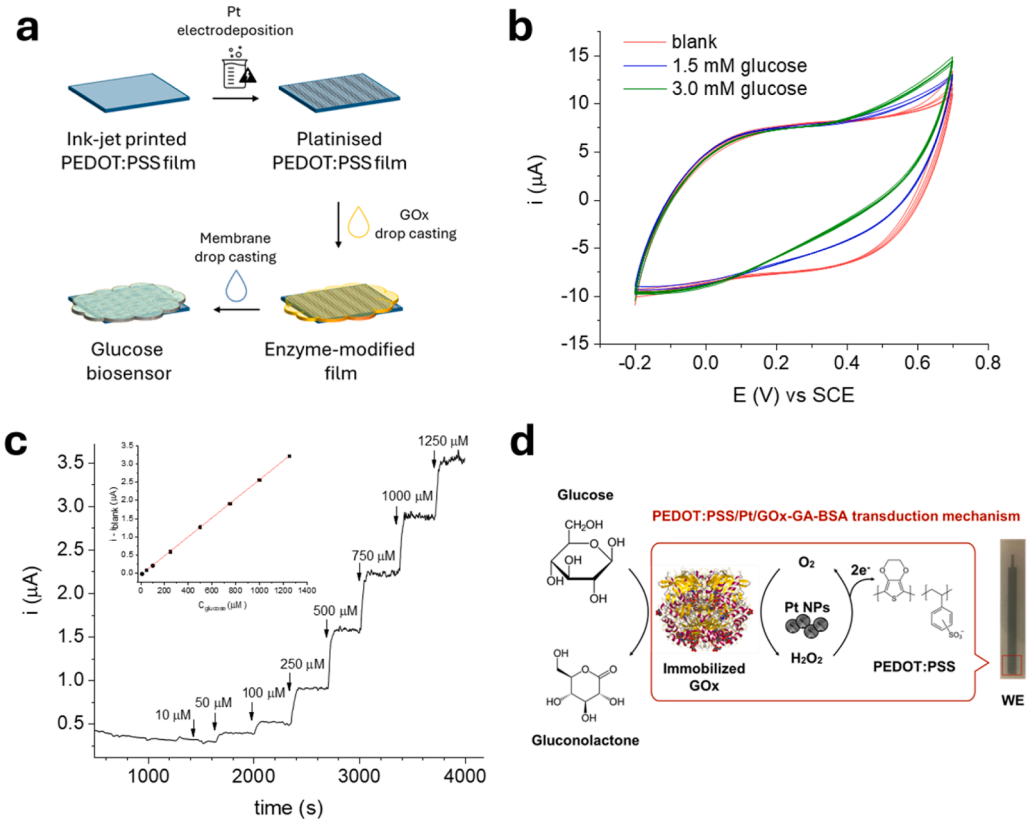


**Fig. 1.** Functionalisation of a printed film for glucose sensing. a) Scheme of the functionalisation procedure optimised on ink-jet printed PEDOT:PSS films. b) Cyclic voltammograms of a glucose biosensor upon glucose additions (scan rate: 50 mV $s^{-1}$). c) Glucose sensing upon application of $E = +0.65$ V vs SCE in 0.1 M PBS, pH 7.00 (Slope: 18 mA $M^{-1}$ $cm^{-2}$; $R^2$ 0.999$_9$), active area 0.15 $cm^2$. d) Proposed sensing mechanism.

The durability of the transducer itself, and therefore of the immobilized enzyme, was investigated during the optimization of the storage conditions. Figure S1 reports a comparison of the sensing performances of a freshly prepared sensor before and after 3 days storage at R.T., and those of a freshly prepared sensor before and after 3 days storage at 4 °C in a refrigerator, inside a closed container with a damp atmosphere. Due to the evident degradation observed in the first case, it was concluded that the transducer stability is maintained only under the selected storage conditions at 4 °C.

Nanostructured Pt films are among the most established electrode modifiers for glucose biosensors, as they increase the electrode surface area as well as electron transfer kinetics. Being excellent amperometric sensors for $H_2O_2$ over a wide range of concentrations, they are particularly relevant to all biosensing applications where $H_2O_2$ is released during the oxidation of a substrate by a specific oxidoreductase in the presence of $O_2$ [19,20]. Therefore, the role of Pt and the effect of its deposition style on the electrode surface were extensively studied. Electrodeposition was carried out from a diluted hexachloroplatinic acid solution comparing potentiostatic and potentiodynamic approaches: the first was realized upon application of −0.2 V vs SCE for 180 s, while in the second the potential was linearly scanned from −0.2 to 0.0 V vs SCE for 100 cycles (scan rate 50 mV/s). Atomic Force Microscopy (AFM) images acquired for the pristine ink-jet printed PEDOT:PSS electrode and two electrodes subjected to potentiostatic and potentiodynamic Pt deposition are reported in Figure S2. From the analysis of the different topographical images, it is clear that, when the potentiodynamic approach is employed, the material surface is not uniform and exhibits clusters of typical dimensions ranging from 100 nm up to 500 nm. On the contrary, when the potentiostatic approach is employed, the PEDOT:PSS-Pt surface is much more homogeneous, thus suggesting an overall superior uniformity of Pt deposition during the functionalization process. The amperometric response of a fully functionalized biosensor modified with potentiodynamically deposited Pt (Figure S3) was acquired in the same experimental conditions as Fig. 1c: the biosensor exhibits lower sensitivity, lower signal-to-noise ratio and smaller linear concentration range than the potentiostatically realized counterpart. Such behaviour well correlates with the scarce uniformity of the potentiodynamic functionalization procedure, as observed from the AFM investigation. For these reasons, the potentiodynamic approach was abandoned. The possibility of using commercially available Pt NPs for electrodes modification was explored as well. Specifically, 10 μL of Pt NPs were drop-cast on the printed PEDOT:PSS surface and, after enzyme immobilization, the biosensor was tested by amperometry upon glucose additions (Figure S4). Due to the signal drift hindering the achievement of steady state conditions, this data could not be further analysed. Moreover, the scarce repeatability between two subsequent tests suggests a high instability of the biosensors prepared using drop-cast Pt NPs. Therefore, this approach was also discarded for further investigations. Once the potentiostatic electrodeposition was selected among the other methods, the role of Pt in promoting charge transfer mechanisms and facilitating glucose detection via $H_2O_2$ oxidation was investigated. The response of PEDOT:PSS/Pt NPs electrodes to $H_2O_2$ is reported in Figure S5. It is worth noting that PEDOT:PSS shows negligible response to the analyte, while the presence of Pt allows analyte detection with higher sensitivity and linear coefficient at +0.65 V than +0.45 V vs SCE. To summarize, the proposed sensing mechanism for the glucose biosensing interface is schematically reported in Fig. 1d, where Pt facilitates the charge transfer between the enzymatically produced $H_2O_2$ and PEDOT:PSS.

### 3.2. Optimisation of the printed electrodes layout

Fabrication aspects play a pivotal role in defining the robustness of electrochemical sensors: though they are evidently associated with production costs and efficiency, they have a large impact on the properties of electrochemical interfaces as well. The active area of the electrodes is made of PEDOT:PSS, while connections and pads are made of Ag in order to ensure high conductivity, thus reducing voltage decay along longer distances. The sensing area, i.e. the PEDOT:PSS surface to be exposed to test solution, is defined by a patterned Parylene C (PaC) encapsulation layer, which covers all connecting lines to avoid their direct interaction with the measurement environment (Fig. 2a). Electrochemical characterizations (Fig. 2b) revealed the dramatic impact of the positioning of the contact point between PEDOT:PSS and Ag: only by moving upward this interface (from generation 1 to 2 layout in Fig. 2a), we were able to obtain a stable electrochemical signal without unwanted faradaic peaks ascribable to the metal. We hypothesise that this adjustment is crucial to keep the electrolyte solution away from Ag, despite the swelling properties of the organic semiconductor. Another important fabrication element that was optimized based on the final sensing performance regards the final step, where PaC is etched to dig the underlying active area of PEDOT:PSS out. We realized that the etching process not only removes the insulator, but also it is likely to damage the surface of the PEDOT film via overoxidation. Fig. 2c-d prove that reprinting a new layer of PEDOT:PSS on the active area after PaC etching significantly improves the sensing performance of the device.

### 3.3. Design and miniaturization of printed amperometric biosensors

After optimization of the functionalization protocol and the printing procedure, we focused on the design and miniaturization of glucose biosensors in the amperometric and transistor configurations. The most evident difference between the two is the reference element, which is characteristic of the amperometric layout. To obtain a stable, miniaturised pseudo-reference electrode, we chose the non-polarizable Ag/AgCl evaluating the options of (i) electrochemically forming AgCl on the surface of a printed Ag ink track (Fig. 3a, top) and (ii) electrochemically depositing Ag, followed by AgCl formation, on the printed PEDOT:PSS film (Fig. 3a, bottom). The stability of the two pseudo-REs was initially assessed upon acquisition of their open circuit potential versus a calomel electrode for 2 h in 0.1 M PBS, pH 7.00 (data not shown). The Ag-Ink/AgCl electrode stabilised to an average value of +0.202 V vs SCE, with a relative drift of 1.39 %/h, while the PEDOT:PSS/Ag/AgCl pseudo-RE, stabilised to a similar potential value (+0.199 V vs SCE), but showed a higher relative drift of 3.69 %/h. In order to take into account these potential shifts with respect to the bulk SCE, +0.45 V was the electrochemical potential of choice for the fully integrated biosensors. However, when analysing the amperometric responses to glucose upon application of +0.45 V vs each pseudo reference electrode (Fig. 3b, c), the biosensor comprising the Ag-Ink/AgCl pseudo-RE performed worse than its counterpart based on the PEDOT:PSS/Ag/AgCl pseudo-RE. In fact, a higher noise affects the steady state current across the whole concentration range, resulting also in lower slope and linearity of the

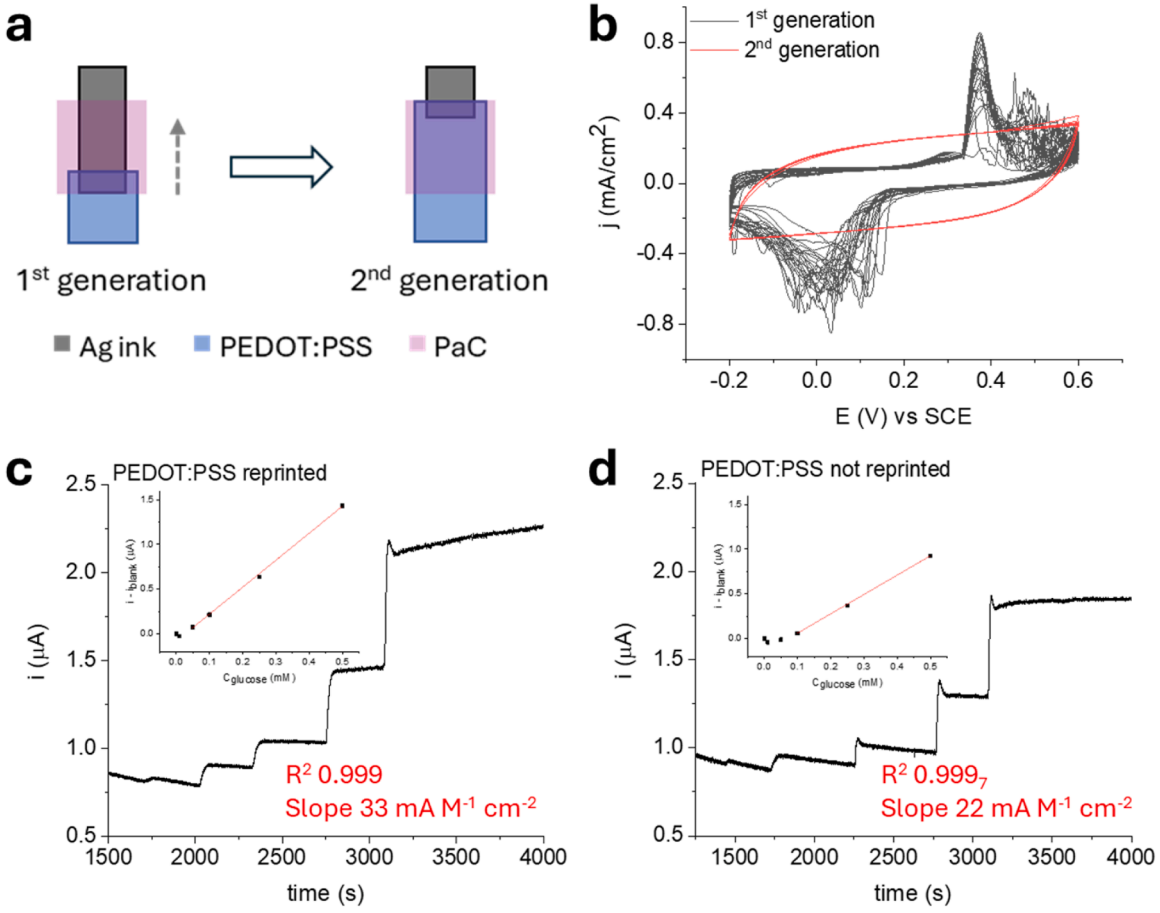


**Fig. 2.** Optimization of the electrodes design. a) Adjustment of the Ag ink-PEDOT:PSS electric contact positioning. b) Voltammograms of printed PEDOT:PSS electrodes before (1st gen) and after (2nd gen) optimization of the electrodes design. 0.1 M PBS pH 7.00; scan rate 50 mV $s^{-1}$. Amperometric response of two biosensors prepared using 2nd generation electrodes with (c) reprinted and (d) not reprinted PEDOT:PSS after PaC etching (0.09 $cm^2$ area), upon application of +0.65 V vs SCE during glucose additions to a 0.1 M phosphate buffer solution. Correspondent calibration curves are reported as insets. Glucose additions: 0.01; 0.05; 0.10; 0.25; 0.50 mM.

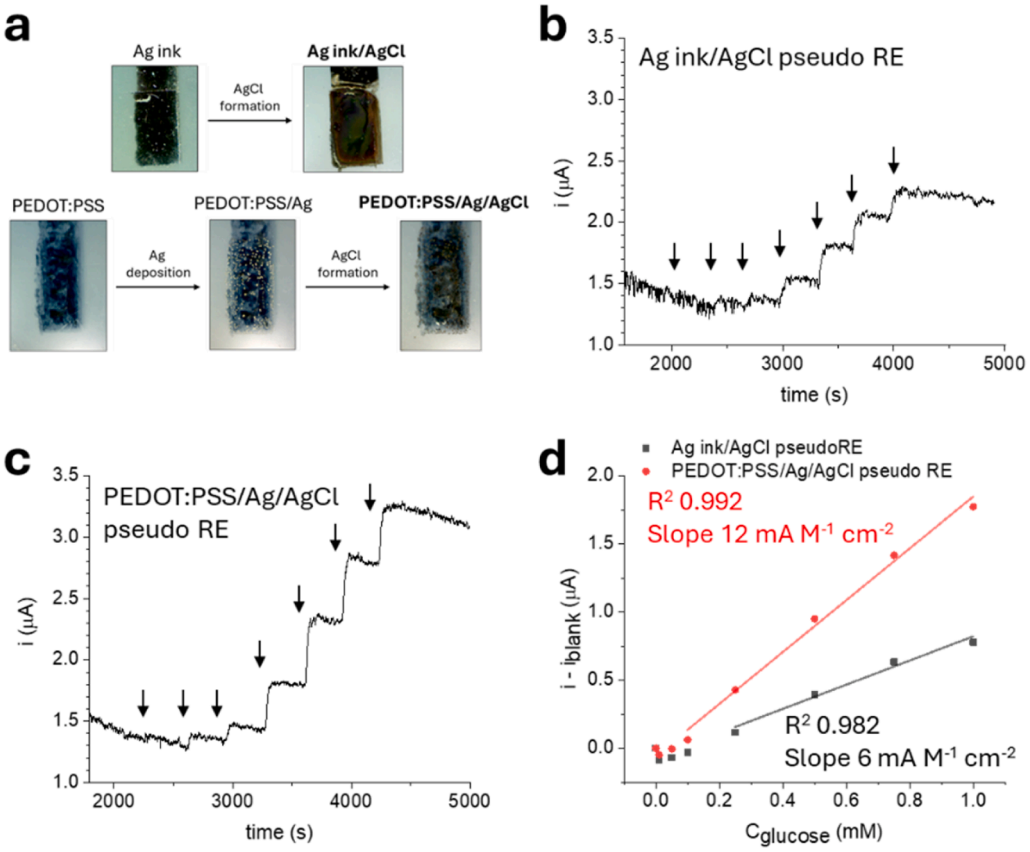


**Fig. 3.** Formation of the pseudo reference electrode. (a) Schematics of the steps involved in the formation of Ag ink/AgCl (top) and PEDOT:PSS/Ag/AgCl (bottom) pseudoREs. Amperometric response of two biosensors recorded upon application of $E = +0.45$ V vs (b) Ag ink/AgCl pseudoRE and (c) PEDOT:PSS/Ag/AgCl pseudoRE. Corresponding calibration curves are shown in (d). Glucose additions: 0.01; 0.05; 0.10; 0.25; 0.50; 0.75; 1.0 mM. Electrodes area: 16 $mm^2$.

calibration curve (Fig. 3d). For these reasons, the PEDOT:PSS/Ag/AgCl pseudo-RE was selected for further measurements. Notably, extended stability measurements over about 22 h against a double junction SCE in the presence of a small chloride concentration (0.1 mM) showed a much lower drift for this electrode, decreasing to 0.05 %/h.

Once all sensor elements were defined, the impact of device miniaturization on the analytical performance was systematically investigated. In particular, the sensor size was downscaled across two generations of devices, as illustrated in Fig. 4a.

The response of a generation A amperometric sensor, with active WE area of 0.16 $cm^2$ (WE) , is presented in Figure S6. The generation A sensor exhibits a sensitivity of 11 mA $M^{-1}$ $cm^{-2}$ in its linear range from 0.01 to 1 mM glucose; however, the reproducibility in terms of relative standard deviation (RSD) of the sensitivity values found within the generation A batch was low and equal to 74 % ($N = 3$). Generation B sensors demonstrated the best analytical characteristics (Fig. 4b, c). With an active WE area of 0.01 $cm^2$, a linear response was obtained in the whole concentration range under investigation, reaching a sensitivity of 43 mA $M^{-1}$ $cm^{-2}$ (Fig. 4b and Test 1 in Fig. 4c) and a LOD of 18 μM. During repeatability studies, sensor degradation was found to significantly reduce the sensitivity (19 and 13 mA $M^{-1}$ $cm^{-2}$ for Test 2 and 3 in Fig. 4c, respectively) and the linear coefficient of the calibration curve. Compared to generation A, the RSD of the sensitivity values found within this batch was significantly improved to 40 % ($N = 3$).

### 3.4. *Design and miniaturization of printed organic electrochemical transistor-based biosensors*

The optimized biosensing interface was also realized on the gate electrode of ink-jet printed OECTs, with the scope to highlight limitations and advantages of a referenceless sensing layout. In analogy with the amperometric sensors, the impact of device miniaturization on the analytical performance was investigated for the transistor-based sensors as well. Also in this case, the sensor size was downscaled across two generations of devices, as illustrated in Fig. 5a.

Importantly, the electrochemical behaviour of the transistor elements, as well as the influence of Ag/Ach (γ), where Ag and Ach are the gate and channel geometric areas, respectively, was investigated within generation A devices. To do so, OECT biosensors having γ equal to 0.21, 0.43 and 0.64 were fabricated by changing the gate size (see Fig. 5a), while maintaining a fixed GOx loading on the gate electrode of 1.7 GOx units/$mm^2$ and a fixed channel area. Therefore, operando recordings of the electrochemical potentials of gate (Eg), source (Es) and drain (Ed) with respect to a reference electrode were carried out [14,21] in order to find the appropriate working voltages and γ value for transistor operation as a glucose sensor (Figure S7). The trends of Eg, Es and Ed are in agreement with the behaviour of a depletion mode OECT, where holes extraction occurs in the channel at positive Vg [22]. By comparing the data obtained in buffer solution (solid squares) and in the presence of 400 μM glucose (hollow circles), no significant shift of the electrochemical potentials (ΔE between the two sets of data) can be detected in the device with the smallest γ value (0.21). In particular, no evident impact on the modulation of Es and Ed (regulating the channel conductivity [22]) can be ascribed to the occurrence of glucose oxidation at the gate at sufficiently high Vg values. Moreover, the modulation of the electrochemical potential of the channel in the presence of the analyte is higher for the middle geometry (γ = 0.43) than the larger one (γ = 0.64), suggesting that the pseudo-capacitive contribution is dominant in the bigger gate electrode, rather than the faradaic contribution due to the enzymatic reaction. Measurements carried out at different Vd (−0.1,

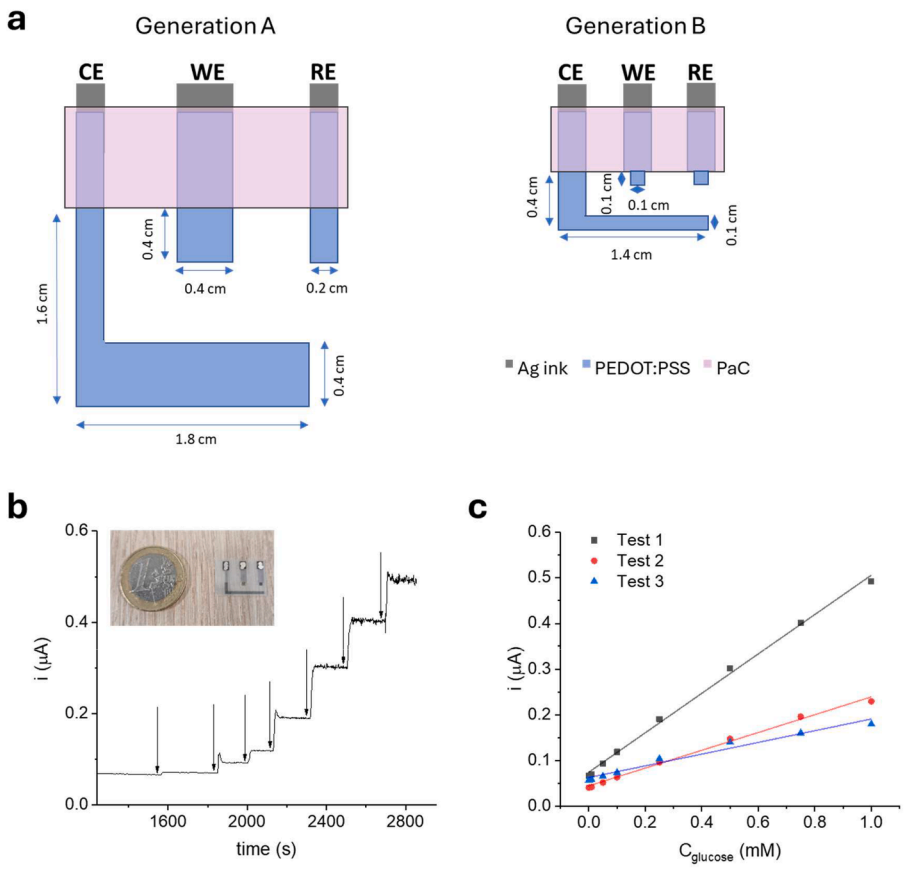


**Fig. 4.** Miniaturisation of printed amperometric biosensors. a) Scheme of the two generations of amperometric biosensors. Total device area was about 6 $cm^2$ and 1.7 $cm^2$ for generation A and B, respectively. b) Amperometric response of a generation B biosensor, recorded upon application of $E = +0.45$ V vs its PEDOT:PSS/Ag/AgCl pseudoRE. Inset: picture of the generation B biosensor. c) Corresponding calibration curve (test 1, $R^2 = 0.997$) including repeatability measurements (test 2, $R^2 = 0.994$, and test 3, $R^2 = 0.972$). Glucose additions: 0.01; 0.05; 0.10; 0.25; 0.50; 0.75; 1.0 mM.

−0.2 and −0.3 V, data not reported) showed negligible influence on the recorded electrochemical potentials. These considerations support the comparison among the sensing performance exhibited by the three investigated geometries (Figure S8). In particular, evident difficulty in reaching a steady state during glucose additions is observed for the smallest and for the biggest gate area. Specifically, the smallest gate area cannot induce sufficient modulation on Id, which just drifts without showing any stepwise behaviour and never reaches a steady state. In turn, the larger gate area leads to some stepwise modulation on Id despite the drift, however a linear relation could not be obtained between Id and the glucose concentration, suggesting that the observed modulation is mainly due to pseudo-capacitive phenomena. This finds explanation in the literature reporting about the influence of γ on the performance of all-PEDOT:PSS OECT sensors, where the gating effect dominates the transistor response rather than faradaic reactions involved in analytes sensing when large gate electrodes are used [23]. Differently, the mid-γ value OECT (0.43), which exhibits the most evident ΔE, is also the only geometry showing a clear steady-state behaviour of Id upon glucose additions, reaching a sensitivity of 13 mA $M^{-1}$ in the range 0.05 - 1 mM ($R^2$ 0.996). Although the detection relies on the same faradaic reaction taking place at the WE of the amperometric sensors and at the gate of the OECTs, whose surfaces share the same functionalization, the transduction mechanism is rather different. The analytical signal in the OECT sensor is in fact the Id, which decreases as glucose concentration increases and a larger Ig flows. Lastly, the effect of gate positioning relative to the channel (centred, closer) on the sensing performance was found to be negligible (data not shown). Based on all these observations, we can conclude that (i) a γ value of about 0.3–0.4 seems to make the transduction mechanism more efficient from an electrochemical point of view and (ii) a Vg of +0.80 V should guarantee a sufficiently oxidizing gate interface (e.g., assuming a sufficiently high E) for glucose detection.

Following the characterization of this first OECT biosensor prototype, the miniaturized generation B was produced with a γ of 0.29. Concerning the electrical behaviour, Figure S9 reports the I-V characteristics of generations A and B OECTs: the output and transfer characteristics highlight the expected Id-Vd response at different gate voltages (ranging from −0.5 to 0.6 V) and Id-Vg response, respectively, for an all-PEDOT:PSS OECT operating in depletion mode, where positive gate voltages cause the overall reversible reduction of the channel material, with the consequent decrease of Id [22,24]. As regards the sensing performance, OECT B biosensors response is reported in Fig. 5b,c. A linear response was obtained in the whole concentration range under investigation (0.01–1 mM), reaching a sensitivity of 12 mA $M^{-1}$ (Fig. 5b and Test 1 in Fig. 5c) and a LOD of 66 μM. During repeatability studies, a decrease in the obtained sensitivity values was observed (8 mA $M^{-1}$ for both Test 2 and 3). The RSD of the sensitivity values found within this batch (7 %, $N = 3$) resulted largely improved in comparison to gen. A (22 %, $N = 3$), and this improvement was accompanied by a reduced variability in the channels resistance (from 18 % for gen. A to 8 % for gen. B). The durability of the final miniaturized sensors was characterized over a period of 7 days, during which the device was stored in the optimized conditions (4 °C, damp atmosphere). Figure S10 reports the calibration curves obtained from two different OECT miniaturized sensors belonging to the same fabrication batch, the first being used as prepared, while the second being tested 7 days after preparation. The small difference in the two sensitivity values ($7 \times 10^{-4}$ and $8 \times 10^{-4}$ $\mu M^{-1}$ for the freshly tested OECT 1 and for the stored OECT 2, respectively) can be

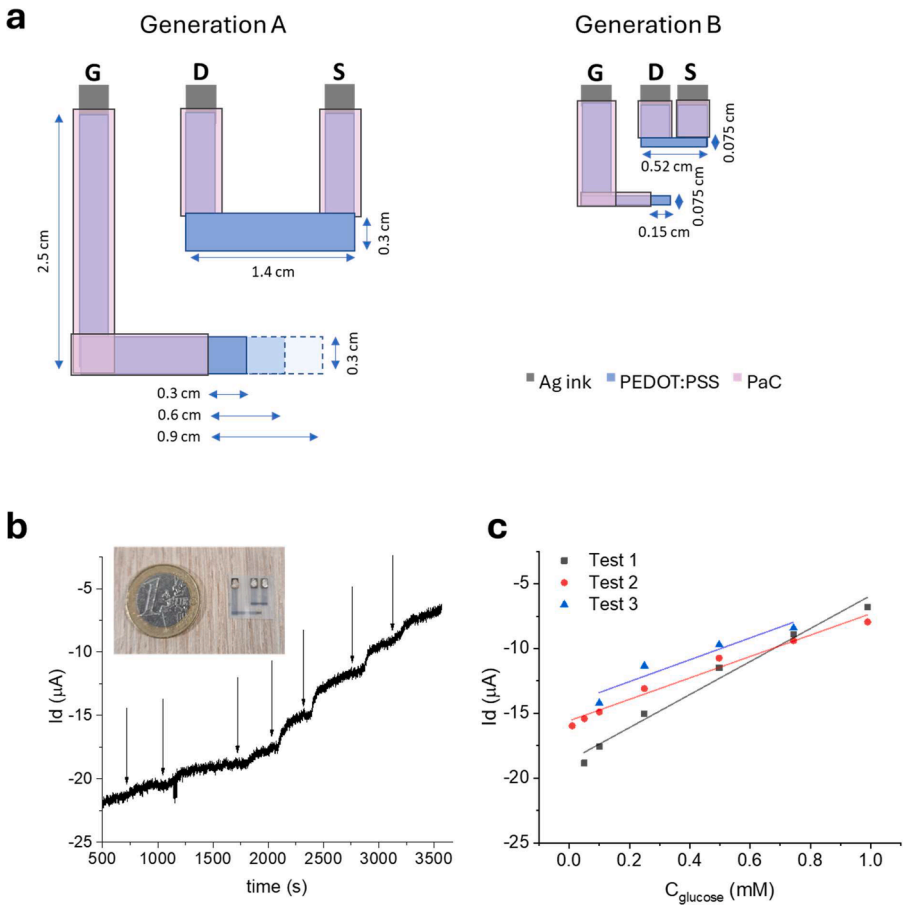


**Fig. 5.** Miniaturisation of printed OECT biosensors. a) Scheme of the two generations of OECT biosensors. Total device area was about 5 $cm^2$ and 1.2 $cm^2$ for generation A and B, respectively. b) Potentiostatic response of a gen. B biosensor, recorded upon application of Vg = +0.8 and Vd = −0.2 V. c) Corresponding calibration curve (test 1, $R^2 = 0.980$) including repeatability measurements (test 2, $R^2 = 0.978$ and test 3, $R^2 = 0.913$). Glucose additions: 0.01; 0.05; 0.10; 0.25; 0.50; 0.75; 1.0 mM.

ascribed to intra-batch variabilities.

As far as mechanical flexibility is concerned, the OECT channel resistance was monitored during 40 bending cycles where the device was curved around a 1.5 cm diameter cylinder, resulting in a bending angle of about 90°. Fig. 6 shows the behavior of an OECT bent parallel and an OECT bent transversely to its channel, causing an overall variation in the channel resistance of 0.8 and 0.3 %, respectively, thus demonstrating excellent robustness to mechanical stress [25,26].

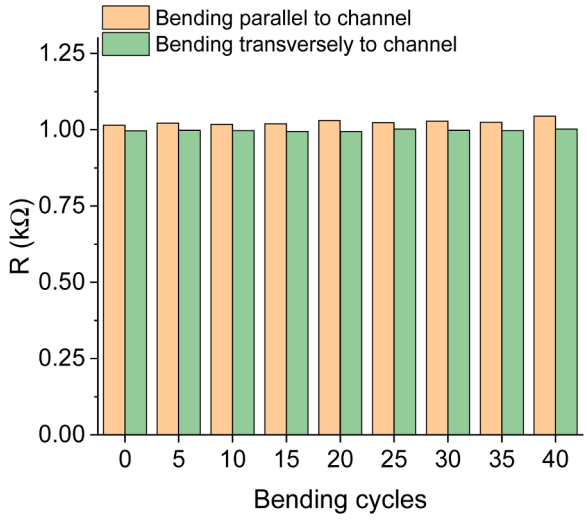


**Fig. 6.** Device flexibility. Effect of 40 bending cycles on the channel resistance of two flexible OECTs.

### 3.5. Selectivity

Interference studies were carried out using the final, miniaturized amperometric and OECT biosensors (gen. B), which led to analogous results. We report in Fig. 7 representative measurements obtained with an OECT biosensor. Paracetamol was chosen by virtue of its ease of oxidation at PEDOT:PSS electrodes [27] and because it is the most common pharmacologic source of interference for CGM devices [28]. Considering the concentration range found in plasma and ISF after ingestion of a normal dose of a commercial drug [28], no interference on the analytical signal was detected (Fig. 7a). Possible interference arising from lactic acid was also evaluated (Fig. 7b), as lactate is produced during glucose metabolism and it is present in the majority of biofluids [29]. No interference was detected within the same concentration range of glucose investigated in this work.

Furthermore, the potential interference of other biomarkers found in human biofluids like saliva and sweat was evaluated [30,31]. Specifically, (i) chloride ion, i.e. the most abundant anion in bodily fluids, (ii) urea, (iii) albumin, to take into account the protein content, (iv) ascorbic acid (AA) and (v) uric acid (UA) were tested. While $Cl^-$, urea and albumin caused a signal interference smaller than 3 %, the interference of AA and UA on the analytical signal was 19 % and 30 %, respectively, at the examined concentrations. This result is coherent with the excellent performance of PEDOT:PSS-based sensors and OECTs in the detection of

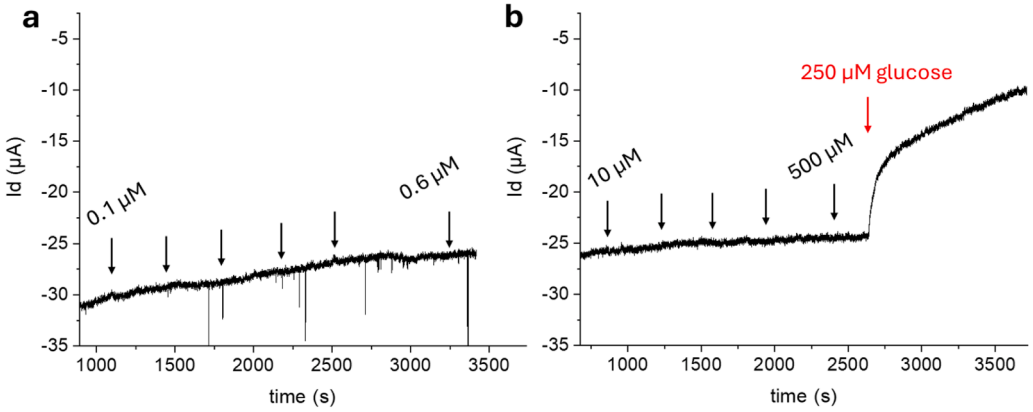


**Fig. 7.** Effect of paracetamol and lactic acid. a) Id vs time curve recorded during paracetamol additions (0.1, 0.2, 0.3, 0.4, 0.5, 0.6 μM) to 0.1 M PBS (pH 7.00). b) Id vs time curve recorded during lactic acid additions (10, 50, 100, 250, 500 μM) to 0.1 M PBS (pH 7.00).

easily oxidizable molecules [21,24]. In this case, the interference likely arises from AA and UA electrooxidation at the gate/solution interface due to the applied potentials chosen for glucose detection, thus causing holes extraction from the OECT channel and the following Id variation.

## 4. Discussion

Thanks to the analogy between the OECT and amperometric biosensors developed in this work in terms of fabrication procedure, functionalization, employed materials and operative conditions, a fair and consistent comparison of the resulting performances can be carried out. Within the investigated concentration range (0.01 – 1 mM glucose), both sensors exhibit a linear response with absolute sensitivities (without WE or gate area normalization) of 0.43 and 12 mA $M^{-1}$ for the amperometric sensor and the OECT, respectively, thus demonstrating the amplification provided by the transistor structure. The higher sensitivity combined with the higher intensity of the analytical signal (the drain current is about 2 orders of magnitude higher than the amperometric current) make the transistor particularly appealing for applications requiring simple, low-power electronics. Nevertheless, the absence of a (pseudo) reference element is likely to produce the observed drift in Id, which, together with the lower S/N ratio compared to the amperometric sensor (72 vs 242, respectively, for the OECT and the amperometric sensor at 250 μM glucose), negatively impacts on the LOD of the OECT. The calculated LOD values for the OECT and the amperometric sensor are 66 and 18 μM, respectively. Still, the linear response of both sensors is consistent with the glucose monitoring in naturally secreted biofluids like saliva, sweat and tears [1,2], as well as extracted ISF [32,33]. However, in light of the interference of easily oxidizable molecules highlighted by the selectivity study, the glucose biosensors should be further modified to improve its robustness: a possible strategy could be the optimization of a Nafion coating on the gate electrode, in order to hinder the diffusion of the negatively charged interferents, such as AA and UA at physiological pH.

With regard to other state-of-the-art ink-jet printed glucose biosensors, our miniaturized devices combine superior analytical performance with a compact layout. Concerning the amperometric sensor, the only fully printed example reported to date lacks details about the main analytical figures of merit and cannot be considered for quantitative comparison [13]. If the work by Setti et al. [12] is considered, where only the working electrode was ink-jet printed on a rigid substrate, our amperometric sensor exhibits higher sensitivity at a lower applied potential (e.g., 43 mA $M^{-1}$ $cm^{-2}$ at +0.45 V vs pseudoRE in this work vs. 6.43 μA $M^{-1}$ $cm^{-2}$ at +0.60 V vs SCE in the work by Setti et al.). Focusing on the OECT biosensor, it shows a linear response over the whole concentration range up to 1 mM glucose, while logarithmic responses are usually reported [17,18] leading to inherently lower sensitivities. This behavior at low glucose concentrations agrees with our previous findings [34] where we discuss the existence of a concentration dependent double regime. As already pointed out in the introduction, only one example of ink-jet printed OECT biosensor has been reported to date with a fully integrated architecture comprising the immobilized enzyme [18]. Table 1 is provided in order to facilitate the discussion among the existing ink-jet printed OECT biosensors for glucose detection. Due to the promiscuous response regimes and in order to give a quantitative comparison among the different sensitivities, we have calculated the normalized current response ( % NCR) as $(1 - I/I_0) \times 100$ at three glucose concentrations that are relevant for non-invasive monitoring. Despite the more limited concentration range, our device offers the highest signal variation at the lowest applied potentials.

## 5. Conclusion

Real-time glucose monitoring in naturally secreted or minimally/non-invasively collected biofluids is one of the most intriguing and potentially high-impact research areas in the field of wearable sensors and point-of-care technologies. In this work, we investigated the advantages and limitations of two different biosensing structures - amperometric sensors and organic electrochemical transistor (OECT) sensors - fully fabricated by ink-jet printing on flexible substrates. By optimizing fabrication and functionalization strategies in parallel with device miniaturization, we developed efficient biosensors for real-time detection within a relevant physiological concentration range, showing superior analytical performance and more compact layout compared to other ink-jet printed, flexible glucose sensors. Notably, the entire production process was conceived to be compatible with flexible substrates and potentially applicable to future on-body applications, as it relies on material-efficient and highly versatile approaches, like ink-jet printing, electrodeposition and drop-casting, as well as low-cost, solution-processable inks and biocompatible materials. Moreover, the direct comparison between the two widely studied sensing architectures for bioelectronic devices offers critical insights for future integration with portable electronics enabling the development of multisensing platforms.

## CRediT authorship contribution statement

**Federica Mariani:** Writing – review & editing, Writing – original draft, Supervision, Project administration, Formal analysis, Data curation, Conceptualization. **Francesca Ceccardi:** Writing – review & editing, Writing – original draft, Methodology, Investigation, Formal analysis. **Giulia Casula:** Writing – review & editing, Writing – original draft, Methodology, Investigation, Formal analysis. **Andrea Falchi:**

**Table 1**
Ink-jet printed OECT biosensors for glucose detection.

| Sensing conditions | Gate and channel materials | Vg, Vd (V) | % NCR, 50 μM glucose | % NCR, 250 μM glucose | % NCR, 750 μM glucose | Concentration range (mM) | Ref. |
|---|---|---|---|---|---|---|---|
| Enzyme **in solution** | C black, PEDOT:PSS | +0.7, −0.8 | 9 % | 11 % | 13 % | 0.001 - 100 | [17] |
| Enzyme and redox mediator **in solution** | Graphene, PEDOT:PSS | +1.0, −0.4 | 27 % | 40 % | 50 % | 0.03 - 5 | [18] |
| Enzyme and ferrocene **immobilized** around the gate electrode | Graphene, PEDOT:PSS | +1.0, −0.4 | 9 % | 15 % | 20 % | 0.03 - 5 | [18] |
| Enzyme **immobilized** on the gate electrode | PEDOT:PSS with electrodeposited Pt, PEDOT:PSS | +0.8, −0.2 | 8 % | 35 % | 75 % | 0.07 - 1 | This work |

Writing – original draft, Methodology, Investigation, Formal analysis. **Luca Sartorelli:** Writing – review & editing, Writing – original draft, Methodology, Investigation, Formal analysis. **Giulia Costa:** Writing – original draft, Formal analysis. **Isacco Gualandi:** Writing – review & editing, Supervision, Funding acquisition, Data curation, Conceptualization. **Piero Cosseddu:** Writing – review & editing, Supervision, Investigation, Funding acquisition. **Annalisa Bonfiglio:** Writing – review & editing, Supervision, Resources, Project administration, Funding acquisition, Conceptualization. **Stefano Lai:** Writing – review & editing, Supervision, Project administration, Funding acquisition, Formal analysis, Conceptualization. **Erika Scavetta:** Writing – review & editing, Supervision, Project administration, Funding acquisition, Conceptualization.

## Declaration of competing interest

The authors declare that they have no known competing financial interests or personal relationships that could have appeared to influence the work reported in this paper.

## Acknowledgments

The authors acknowledge the Italian Ministry of University and Research for funding this research activity under the PRIN 2020 project GLUCOMFORT (A noninvasive tattoo-based continuous GLUCOse Monitoring electronic system FOR Type-1 diabetes individuals).

## Supplementary materials

Supplementary material associated with this article can be found, in the online version, at doi:10.1016/j.snr.2026.100464.

## Data availability

Data will be made available on request.

## References

[1] B. Zhu, X. Li, L. Zhou, B. Su, An overview of wearable and implantable electrochemical glucose sensors, Electroanalysis 34 (2022) 237–245, https://doi.org/10.1002/elan.202100273.
[2] D. Tonelli, I. Gualandi, E. Scavetta, F. Mariani, Focus review on nanomaterial-based electrochemical sensing of glucose for health applications, Nanomaterials 13 (2023) 1883, https://doi.org/10.3390/nano13121883.
[3] S.Sh.M. Ameen, K.M. Omer, F.R. Mansour, A. Bedair, M. Hamed, Non-invasive wearable electrochemical sensors for continuous glucose monitoring, Electrochem. Commun. 173 (2025) 107894, https://doi.org/10.1016/j.elecom.2025.107894.
[4] T. Saha, R. Del Caño, K. Mahato, E. De la Paz, C. Chen, S. Ding, L. Yin, J. Wang, Wearable electrochemical glucose sensors in diabetes management: a comprehensive review, Chem. Rev. 123 (2023) 7854–7889, https://doi.org/10.1021/acs.chemrev.3c00078.
[5] Z. Boeva, Z. Mousavi, T. Sokalski, J. Bobacka, Recent trends in non-invasive on-body chemical sensing, TrAC Trends Anal. Chem. 172 (2024) 117542, https://doi.org/10.1016/j.trac.2024.117542.
[6] J. Kim, A.S. Campbell, J. Wang, Wearable non-invasive epidermal glucose sensors: a review, Talanta 177 (2018) 163–170, https://doi.org/10.1016/j.talanta.2017.08.077.
[7] J. Song, H. Liu, Z. Zhao, P. Lin, F. Yan, Flexible organic transistors for biosensing: devices and applications, Adv. Mater. 36 (2024), https://doi.org/10.1002/adma.202300034.
[8] M. Sophocleous, L. Contat-Rodrigo, E. Garcia-Breijo, J. Georgiou, Organic electrochemical transistors as an emerging platform for bio-sensing applications: a review, IEEE Sens. J. 21 (2021) 3977–4006, https://doi.org/10.1109/JSEN.2020.3033283.
[9] L. Li, L. Pan, Z. Ma, K. Yan, W. Cheng, Y. Shi, G. Yu, All inkjet-printed amperometric multiplexed biosensors based on nanostructured conductive hydrogel electrodes, Nano Lett 18 (2018) 3322–3327, https://doi.org/10.1021/acs.nanolett.8b00003.
[10] D. Panáček, M. Urban, A. Silvestri, I. Dědek, M. Nalepa, A. Merkoçi, M. Prato, M. Otyepka, Nanomaterial-based inkjet printing for electrochemical sensing, Small 22 (2026) e13028, https://doi.org/10.1002/smll.202513028.
[11] S. Han, H. Peng, Q. Sun, S. Venkatesh, K. Chung, S.C. Lau, Y. Zhou, V.A.L. Roy, An overview of the development of flexible sensors, Adv. Mater. 29 (2017), https://doi.org/10.1002/adma.201700375.
[12] L. Setti, A. Fraleoni-Morgera, B. Ballarin, A. Filippini, D. Frascaro, C. Piana, An amperometric glucose biosensor prototype fabricated by thermal inkjet printing, Biosens. Bioelectron. 20 (2005) 2019–2026, https://doi.org/10.1016/j.bios.2004.09.022.
[13] E. Bihar, S. Wustoni, A.M. Pappa, K.N. Salama, D. Baran, S. Inal, A fully inkjet-printed disposable glucose sensor on paper, Npj Flex. Electron. 2 (2018) 30, https://doi.org/10.1038/s41528-018-0044-y.
[14] D. Arcangeli, I. Gualandi, F. Mariani, M. Tessarolo, F. Ceccardi, F. Decataldo, F. Melandri, D. Tonelli, B. Fraboni, E. Scavetta, Smart bandaid integrated with fully textile OECT for uric acid real-time monitoring in wound exudate, ACS Sens. 8 (2023) 1593–1608, https://doi.org/10.1021/acssensors.2c02728.
[15] I. Gualandi, M. Marzocchi, A. Achilli, D. Cavedale, A. Bonfiglio, B. Fraboni, Textile organic electrochemical transistors as a platform for wearable biosensors, Sci. Rep. 6 (2016) 33637, https://doi.org/10.1038/srep33637.
[16] I. Gualandi, M. Tessarolo, F. Mariani, T. Cramer, D. Tonelli, E. Scavetta, B. Fraboni, Nanoparticle gated semiconducting polymer for a new generation of electrochemical sensors, Sens. Actuators B Chem. 273 (2018) 834–841, https://doi.org/10.1016/j.snb.2018.06.109.
[17] S. Khan, S. Ali, A. Khan, B. Wang, A. Bermak, Printing sensors on biocompatible substrates for selective detection of glucose, IEEE Sens. J. 21 (2021) 4167–4175, https://doi.org/10.1109/JSEN.2020.3032539.
[18] S. Demuru, C.-H. Huang, K. Parvez, R. Worsley, G. Mattana, B. Piro, V. Noël, C. Casiraghi, D. Briand, All-inkjet-printed graphene-gated organic electrochemical transistors on polymeric foil as highly sensitive enzymatic biosensors, ACS Appl. Nano Mater. 5 (2022) 1664–1673, https://doi.org/10.1021/acsanm.1c04434.
[19] S. Hrapovic, Y. Liu, K.B. Male, J.H.T. Luong, Electrochemical biosensing platforms using platinum nanoparticles and carbon nanotubes, Anal. Chem. 76 (2004) 1083–1088, https://doi.org/10.1021/ac035143t.
[20] J. Xu, M. Fratus, A. Shah, J.K. Nolan, J. Lim, C.H. Lee, M.A. Alam, H. Lee, Impact of microelectrode geometry and surface finish on enzymatic biosensor performance, Electrochim. Acta 509 (2025) 145270, https://doi.org/10.1016/j.electacta.2024.145270.
[21] F. Ceccardi, F. Mariani, F. Decataldo, V. Vurro, M. Tessarolo, I. Gualandi, B. Fraboni, E. Scavetta, A point-of-care, label-free OECT sensor for uric acid detection: validation in human saliva, Electrochim. Acta 519 (2025) 145834, https://doi.org/10.1016/j.electacta.2025.145834.
[22] F. Mariani, F. Conzuelo, T. Cramer, I. Gualandi, L. Possanzini, M. Tessarolo, B. Fraboni, W. Schuhmann, E. Scavetta, Microscopic determination of carrier density and mobility in working organic electrochemical transistors, Small 15 (2019) 1902534, https://doi.org/10.1002/smll.201902534.
[23] I. Gualandi, E. Scavetta, F. Mariani, D. Tonelli, M. Tessarolo, B. Fraboni, All poly (3,4-ethylenedioxythiophene) organic electrochemical transistor to amplify amperometric signals, Electrochim. Acta 268 (2018) 476–483, https://doi.org/10.1016/j.electacta.2018.02.091.
[24] I. Gualandi, M. Marzocchi, E. Scavetta, M. Calienni, A. Bonfiglio, B. Fraboni, A simple all-PEDOT:PSS electrochemical transistor for ascorbic acid sensing, J. Mater. Chem. B 3 (2015) 6753–6762, https://doi.org/10.1039/C5TB00916B.
[25] G. Liu, H. Xu, P. Zhang, Q. Tan, X. Jin, X. Dou, N. Zhao, C. Li, A wearable microfluidic electrochemical sensor integrated with a bio-inspired sweat collector for electrolyte detection and hydration evaluation, Sens. Actuators B Chem. 448 (2026) 139042, https://doi.org/10.1016/j.snb.2025.139042.
[26] C. Li, Y. Liu, G. Liu, Q. Tan, X. Dou, Y. Xie, X. Zhang, Development of a low-cost flexible potentiometric detector and its integrated system for electrochemical

sensing of electrolytes in human sweat, Sens. Actuators Rep. 9 (2025) 100286, https://doi.org/10.1016/j.snr.2025.100286.
[27] J. Zuo, Y. Shen, J. Gao, H. Song, Z. Ye, Y. Liang, S. Zhang, Highly sensitive determination of paracetamol, uric acid, dopamine, and catechol based on flexible plastic electrochemical sensors, Anal. Bioanal. Chem. 414 (2022) 5917–5928, https://doi.org/10.1007/s00216-022-04157-6.
[28] A. Basu, S. Veettil, R. Dyer, T. Peyser, R. Basu, Direct evidence of acetaminophen interference with subcutaneous glucose sensing in humans: a pilot study, Diabetes Technol. Ther. 18 (2016) S2–43, https://doi.org/10.1089/dia.2015.0410. S2-47.
[29] J.-L. Lafuente, S. González, C. Aibar, D. Rivera, E. Avilés, J.-J. Beunza, Continuous and non-invasive lactate monitoring techniques in critical care patients, Biosensors (Basel) 14 (2024) 148, https://doi.org/10.3390/bios14030148.
[30] K. Ngamchuea, K. Chaisiwamongkhol, C. Batchelor-McAuley, R.G. Compton, Chemical analysis in saliva and the search for salivary biomarkers – a tutorial review, Analyst 143 (2018) 81–99, https://doi.org/10.1039/C7AN01571B.
[31] L.T. Rao, C.K. Mandal, F. Patolsky, Body biofluids for minimally-invasive diagnostics: insights, challenges, emerging technologies, and clinical potential, Adv. Heal. Mater. 15 (2026) e03096, https://doi.org/10.1002/adhm.202503096.
[32] C. McCormick, D. Heath, P. Connolly, Towards blood free measurement of glucose and potassium in humans using reverse iontophoresis, Sens. Actuators B Chem. 166–167 (2012) 593–600, https://doi.org/10.1016/j.snb.2012.03.016.
[33] A.J. Bandodkar, W. Jia, C. Yardımcı, X. Wang, J. Ramirez, J. Wang, Tattoo-based noninvasive glucose monitoring: a proof-of-concept study, Anal. Chem. 87 (2015) 394–398, https://doi.org/10.1021/ac504300n.
[34] I. Gualandi, M. Tessarolo, F. Mariani, D. Arcangeli, L. Possanzini, D. Tonelli, B. Fraboni, E. Scavetta, Layered double hydroxide-modified organic electrochemical transistor for glucose and lactate biosensing, Sensors 20 (2020) 3453, https://doi.org/10.3390/s20123453.